J Electroceram (2007) 18:77–85
DOI 10.1007/s10832-007-9011-z

Engineered sintering aids for PbO-based electroceramics

P. Sooksaen · I. M. Reaney · D. C. Sinclair

Received: 27 July 2005 / Accepted: 5 June 2006 / Published online: 10 February 2007

Abstract Borate- and silicate-based glasses that devitrify on heating to form ferroelectric lead titanate have been developed. Their potential for use as sintering aids in PbO-based electroceramics has been evaluated by studying the densification of $PbTiO_3$ (PT) with increasing wt.% addition of glass powder. When ≥3 wt.% of a borate-based glass was added, ≥94% theoretical density was achieved at 1,100 °C but for a silicate-based glass system 10 wt.% glass addition was required to achieve the same density. As the wt.% glass content increased the maximum and room temperature permittivity decreased and there was also a decrease in T_c and the c/a ratio. The decrease in T_c is believed to be due to increased clamping from neighbouring grains as the density of the PT increases. The decrease in maximum and room temperature permittivity is related to the presence of secondary phases.

Keywords Lead titanate · Glass-ceramics · Sintering aids · Dielectric · Impedance spectroscopy

1 Introduction

One of the significant costs in the manufacture of electroceramics is the energy consumed during thermal processing. From this perspective lower sintering temperatures are desirable. Moreover, high sintering temperatures necessitate the use of expensive electrode materials such as platinum and palladium in many co-fired multilayer devices [1]. Finally, there are environmental concerns over PbO volatilization during high temperature sintering. As a result, much attention has been aimed at reducing the sintering temperature of a wide range of electroceramic products such as barium titanate (BT) [2–5] and lead zirconate titanate (PZT). For BT, $PbO–B_2O_3$ and $Bi_2O_3–B_2O_3$ glass sintering aids [6] have been commonly utilized whereas with PZT, Li_2CO_3, Na_2CO_3, Bi_2O_3 [7] and Cu_2O–PbO oxides [1] have been added to reduce sintering temperatures.

$PbTiO_3$ (PT) is a tetragonal perovskite with a c/a ratio of 1.063 at room temperature, which is the largest known for lead-based perovskite compounds. Single crystal data have shown that the relative permittivity, ε_r, obeys the Curie–Weiss law above the Curie temperature, T_c ~490 °C. The large ionic displacements in PT lead to a particularly large spontaneous polarization (>53 μC/cm^2) and strain (c/a ratio= 1.06) at room temperature [8]. PT exhibits large pyroelectric coefficients, low relative permittivity (~100–200) and dielectric properties stable with time, temperature and frequency. However, these excellent properties are not yet fully realised in bulk polycrystalline samples due to difficulty in fabricating undoped PT. PT ceramics microcrack and fracture on cooling below T_c as a result of the large spontaneous strain generated when the structure changes from cubic to tetragonal. Normally, the fabrication of dense PT ceramics is achieved by reducing the spontaneous strain using dopants and/or inhibiting grain growth. The densification occurs with a reduction of c/a ratio which also affects electrical properties. Palkar et al [9, 10] studied Si-doped PT prepared by a co-precipitation technique. Powder samples of PT with different Si contents were hydrostatically pressed into pellets and sintered under different conditions. They found that the presence of Si in PT did not alter its crystal structure and Si was not found to occupy the Pb or Ti sites in the perovskite lattice. Instead, they suggested that Si was dispersed in either

P. Sooksaen (✉) · I. M. Reaney · D. C. Sinclair
Ceramics and Composites Laboratory (CCL),
Department of Engineering Materials,
Sir Robert Hadfield Building, Mappin Street,
Sheffield S1 3JD, UK
e-mail: mtq02ps@shef.ac.uk

Table 1 Compositions and sintering conditions for glass-PT ceramics.

Sintering conditions	Composition					
	wt.% glass A : wt.% PT			wt.% glass B : wt.% PT		
1,100 °C/2 h	10:90	5:95	3:97	10:90	5:95	3:97
1,000 °C/2 h	10:90	5:95	3:97	10:90	5:95	3:97
900 °C/2 h	10:90	5:95	3:97	10:90	5:95	3:97

a glassy matrix or at interstitial lattice positions. In addition, they reported the presence of a non-ferroelectric metastable, pyrochlore phase ($Pb_2Ti_2O_6$). Wright and Francis [11] also reported that Si promotes the formation of a $Pb_2Ti_2O_6$ phase but also concluded that Si diffuses into interstitial sites of the $PbTiO_3$ lattice. More commonly, either CaO [12] or Sm_2O_3 [13, 14] are added to $PbTiO_3$ to inhibit microcracking and fracture on cooling. The defect chemistry associated with these substitutions is poorly understood but T_c and the c/a ratio decrease in each case.

In this work, high ε_r sintering aids based on borate and silicate glasses containing >35 mol% PbO and >24 mol% TiO_2 have been developed. These sintering aids crystallize as PT-based glass-ceramics and the effect of these sintering aids on the microstructure and properties is investigated and their suitability for potential commercial usage assessed.

2 Experimental and characterization

2.1 Processing

Two glass compositions were utilised:

(A) 39PbO–1BaO–25TiO_2–9.8Al_2O_3–24.2SiO_2–1B_2O_3 (mol%)

(B) 39PbO–1BaO–25TiO_2–9.8Al_2O_3–1SiO_2–24.2B_2O_3 (mol%)

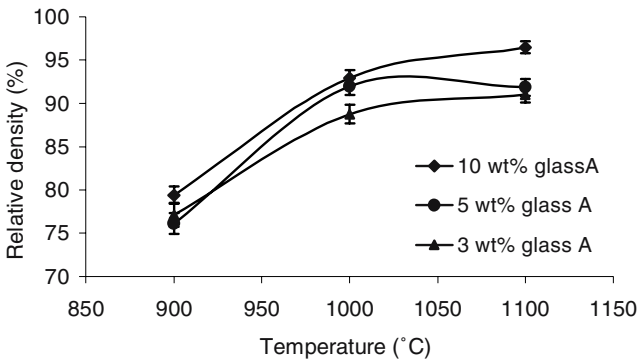

Fig. 1 Density measurements of PT with 3, 5 and 10 wt.% glass A addition, sintered for 2 h between 900 and 1,100 °C

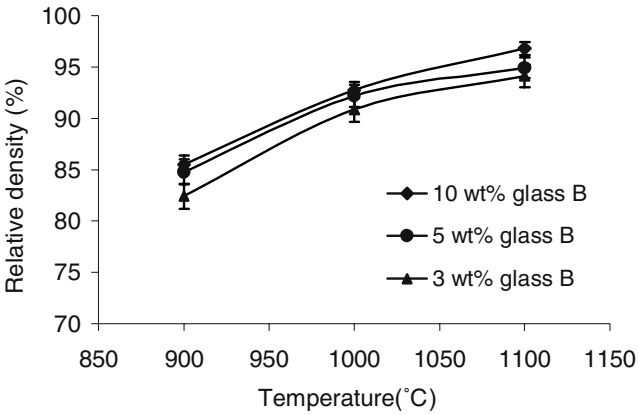

Fig. 2 Density measurements of PT with 3, 5 and 10 wt.% glass B addition, sintered for 2 h between 900 and 1,100 °C

Glass was prepared via rough mixing of the appropriate ratios of Pb_3O_4, $BaCO_3$, TiO_2, $Al(OH)_3$, B_2O_3 and Loch Aline (SiO_2) (all with purity ≥99%) and then transferring the batch to a platinum crucible for melting. Melting was carried out in an electric furnace for 2 h at 1,200–1,250 °C, using a platinum stirrer after 1 h. For glass A, the melt was poured onto a preheated metal block and quickly transferred to a pre-heated muffle furnace for annealing at 500–550 °C for 1 h followed by cooling to room temperature at 3 °C/min. For glass B, cold splatting was used instead of casting as a block in order to retard devitrification.

A solid state mixed oxide route was used to prepare $PbTiO_3$ powder. Mixed powder was calcined at 750 °C/4 h with a 5 °C/min heating and cooling rate. The calcined

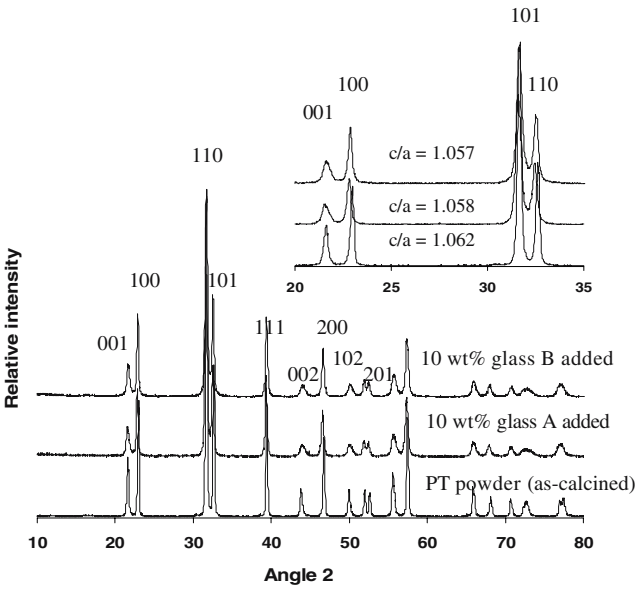

Fig. 3 XRD traces of PT powder (as-calcined) and PT sintered at 1,100 °C/2 h with 10 wt.% glass A and 10 wt.% glass B added. Inset is a magnified image of the XRD with the refined c/a ratios of the PT phase

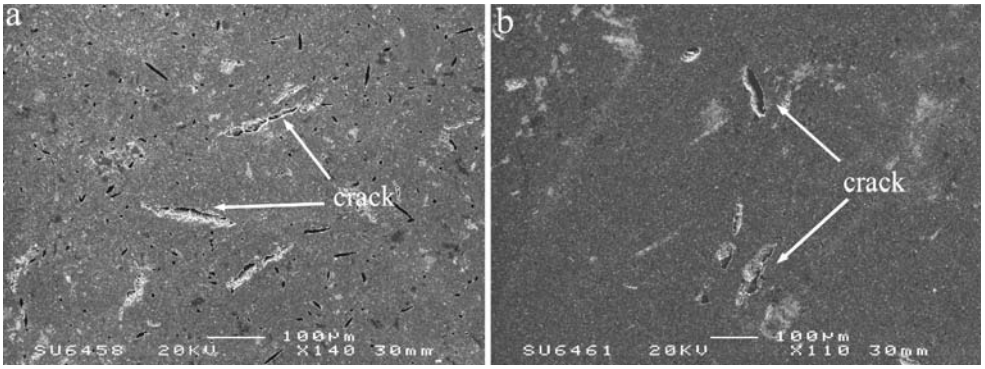

Fig. 4 SEM images of **a** 3 wt. % and **b** 10 wt.% glass A added to PT and sintered at 1,100 °C/ 2 h

powder was then crushed and sieved through 180 μm mesh. Glass A and glass B were crushed in a percussion pestle and mortar and sieved through a 106 μm mesh to yield powder suitable for further ball milling. For each composition, the appropriate amounts (Table 1) of glass A or B and $PbTiO_3$ powder were ball milled for 24 h in distilled water using ZrO_2 milling media. The slurry was then dried and crushed using pestle and mortar and sieved through a 180 μm mesh. Mixed/milled glass and $PbTiO_3$ powders were cold pressed to form pellets using a 10 mm diameter steel die with an applied load of ~125 MPa. The thickness of each green compact was about 2 mm. The green compacts were sintered in air according to the sintering conditions given in Table 1. Sintering was carried out in a lidded crucible with green pellets embedded in PT powder and using a heating and cooling rate of 5 and 2 °C/min, respectively. Density measurements were carried out using the Archimedes technique. The apparent density of the ceramic/glass composites were compared to their theoretical density, assumed to be a summation of the density of the glass and $PbTiO_3$ in appropriate ratios.

2.2 Characterisation

X-ray Diffraction (XRD) was used to identify phases of the sintered pellets. Pellets were crushed and XRD was performed using a Siemens D500, operated at 40 kV and 30 mA, scanned from 10° to 80° with a scan speed of 1°/ min and step interval 0.02° using Cu K_α radiation with a wavelength of λ=1.5406 Å. The samples were first calibrated with a Si internal standard to eliminate errors due to detector misalignment. Lattice parameters of $PbTiO_3$ were calculated from a least squares programme against XRD traces of the $PbTiO_3$ phase. The data were analyzed using Stoe WinXPow (v.2.1) software. Microstructural analysis was carried out using a JEOL JSM6400 SEM and a Philips EM420 TEM operated at 20 and 200 kV, respectively. Samples for SEM were prepared by grinding and polishing as-sintered pellets to a depth of 0.5 mm, followed by thermal etching for 30 min at 100 °C below their sintering temperatures. Samples were prepared for the TEM using conventional grinding and ion thinning techniques. Samples were thinned until perforation using a Gatan Duo Mill, operating a combined gun current of 0.6 mA, an accelerating voltage of 6 kV and an incidence angle of ~12°. Qualitative chemical analyses were obtained by Energy Dispersive X-ray (EDS) spectroscopy on both the JSM 6400 SEM and the EM420 TEM.

Dielectric properties as a function of temperature were obtained using an HP 4284A, LCR meter connected to a non-inductive wound vertical tube furnace. An accurate determination of the tetragonal-cubic transition temperature, T_c, was obtained using an Agilent 4294A, precision impedance analyzer. Before the measurements, samples

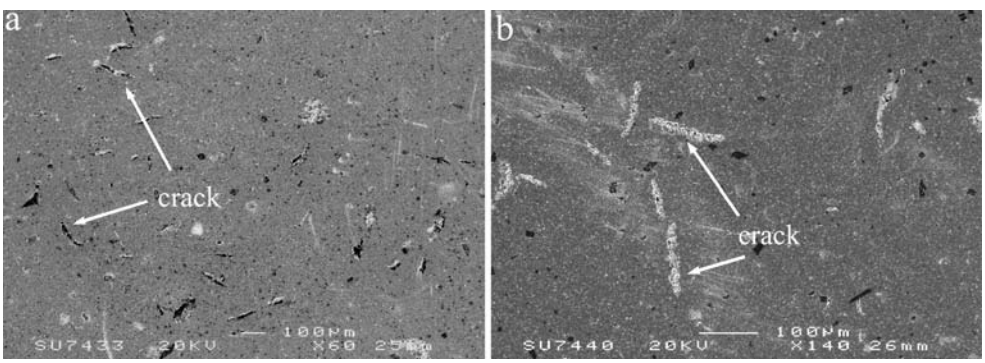

Fig. 5 SEM images of **a** 3 wt. % and **b** 10 wt.% glass B added to PT and sintered at 1,100 °C/ 2 h

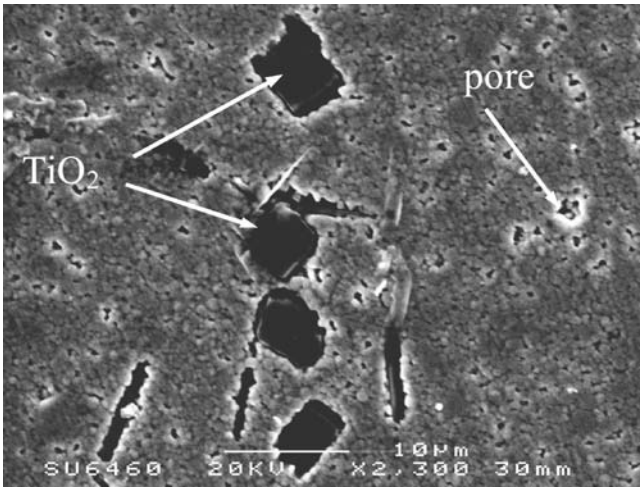

Fig. 6 Higher magnification SEM image of 3 wt.% glass A addded to PT, sintered at 1,100 °C/2 h

were electroded with gold paste on the top and bottom faces. Electrodes were fired at 800 °C for 1 h with a heating rate of 10 °C/min.

Impedance spectroscopy (IS) was used to measure the electrical impedance, Z, of samples as a function of frequency and temperature. Data were collected between 100 Hz to 10 MHz using an Agilent 4294A. The contribution of different electro-active regions to the overall electrical behaviour was then separated. Impedance data were fitted to an equivalent circuit representative of the transport phenomena taking place in the system under investigation. Data were analyzed from four interrelated formalisms; complex impedance, Z^*, admittance, Y^*, permittivity, ε^* and electric modulus, M^* [15, 16], each with real and imaginary components e.g. $Z^* = Z' - jZ''$ and $M^* = M' + jM''$, where $j = \sqrt{-1}$. For an equivalent circuit consisting of a single R and C connected in parallel Z^* plots exhibit a single arc with a low frequency intercept on the real axis, where $Z' = R$. A corresponding combined Z'' and M'' spectroscopic plot consists of a Debye peak in each formalism. The peaks in Z'' and M'' are expressed as $Z'' = R\left[(\omega RC)/\left(1 + (\omega RC)^2\right)\right]$ and $M'' = (\varepsilon_0/C)\left[(\omega RC)/\left(1 + (\omega RC)^2\right)\right]$, and occur at the same frequency in the case of ideal behaviour. M'' spectra are particularly useful in identifying and characterising bulk behaviour as opposed to grain boundary responses or resistive surface layers [17, 18].

3 Results and discussion

3.1 Ceramic densification

Figures 1 and 2 show the % density obtained at various sintering temperatures with different wt.% addition of glass A and B, respectively. Densities are calculated from that of the glass and the theoretical density of PT. In general, the greater the wt.% of glass the higher was the density at any given temperature. Densities >94% theoretical were achieved for 3, 5 and 10 wt.% additions for glass B and for 10 wt.% addition of glass A at 1,100 °C/2 h. Below 1,100 °C, densities were typically <94% theoretical but unlike conventional ceramic PT, the glass-powder composites did not fracture on cooling after sintering provided >2 wt.% glass was added.

3.2 Phase analysis by XRD

Figure 3 shows XRD traces of pellets that contain 10 wt.% glass addition, sintered at 1,100 °C/2 h and compared with as-calcined $PbTiO_3$ powder. Samples with glass additions give similar XRD traces to that obtained from the as-calcined PT powder with no second phases observed. However, ceramic samples with glass additions showed

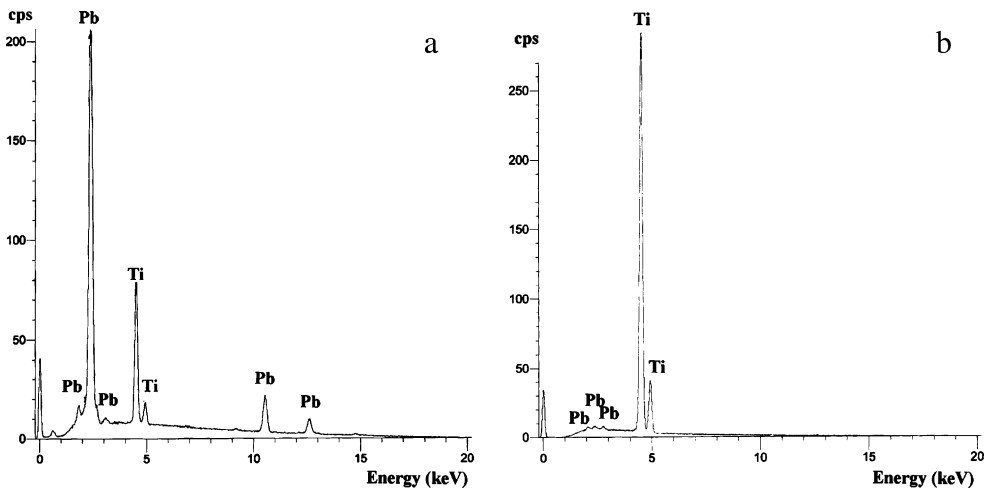

Fig. 7 EDS traces of **a** PT matrix and **b** TiO_2 crystals in Fig. 6

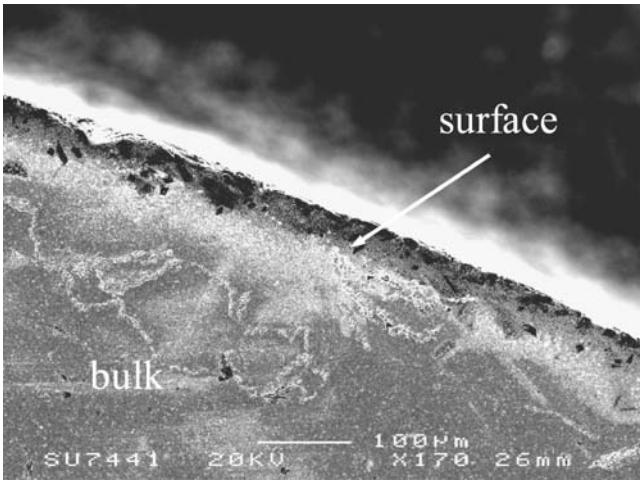

Fig. 8 SEM image of bulk and surface region of 3 wt.% glass A added to PT, sintered at 1,100 °C/2 h

peak broadening associated with a smaller average crystallite size. Inset in Fig. 3 is a magnified view of the {001} and {110} peaks illustrating the c/a ratio for the three compositions. The separation of {hh0} and {h00} is slightly reduced in the glass-PT composites (c/a=1.058 and 1.057 for glass A and B, respectively) with respect to as calcined PT (c/a=1.062). This marginal difference may be due to the incorporation of impurities such as Al, B or Si from the glass into the PT lattice, the residual stress with ceramics or as a result of clamping within the dense PT ceramics that is associated with a smaller average crystallite size. At this stage, clamping within the dense PT ceramics and residual stresses are possible causes of XRD peak broadening but impedance spectroscopy data presented in Section 3.5 indicates that there is no measurable compositional variation in the PT.

3.3 Microstructural analysis

To illustrate typical microstructures, samples sintered at 1,100 °C/2 h with 3 and 10 wt.% glass additions were selected for SEM analysis. Low magnification images, Fig. 4 (glass A) and Fig. 5 (glass B), illustrate that pellets with 10 wt.% glass generally exhibit fewer microcracks compared with 3 wt.%. The crack lengths in all cases are ~100 µm. Between the microcracks however, a similar microstructure was observed in all pellets (Fig. 6) with grain size varying from 0.4–1.0 µm. In addition, some secondary phase (darker contrast in Fig. 6) was observed which was Ti-rich compared with the lighter contrast matrix (Fig. 7). The most likely second phase is therefore TiO_2 rejected from PT phase as a result of PbO loss during reaction or sintering. Figure 8 is a cross section SEM image of a bulk and surface region of a sample with 3 wt.% glass A added to PT, sintered at 1,100 °C/2 h. The darker contrast region at the edge of the sample reveals evidence of PbO volatilisation during sintering.

To study the densification and grain growth, samples with 10% glass A and B were sintered at 1,100 °C for 10 h rather than 2 h. The subsequent SEM images are shown in Fig. 9. After 10 h, there is a bimodal distribution of grain size, indicating the likely presence of liquid phase consistent with the differential thermal analysis data for Glass A presented by Sooksaen et al [19].

Samples with the addition of 10 wt.% glass A and 10 wt.% glass B sintered at 1,100 °C/2 h were selected for further study using TEM to investigate the effect of glass additions on the sintering mechanism(s). Previous work, Sooksaen et al [19, Sooksaen et al., unpublished] has shown that the borate-based glass B, has a lower glass transition temperature (T_g=445 °C) than glass A (silicate-based, T_g=565 °C). In principle therefore, it is anticipated that Glass B additions will flow, enable diffusion or form liquid phase(s) at lower temperatures than Glass A. However, an unpredictable aspect is the degree to which the glass regions in the glass-PT composites 'stiffen' due to crystallisation, potentially inhibiting low temperature sintering.

Figure 10 is a bright field (BF) TEM image of a sample with 10 wt.% glass A added to PT. The image shows a region of glass addition that has crystallized during sintering. The grains (~0.5 µm) containing lamellar

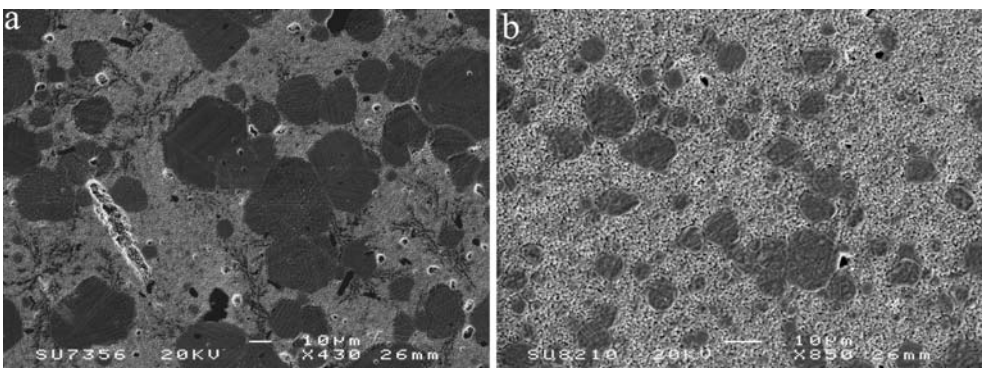

Fig. 9 SEM images of samples sintered for 10 h; **a** 10 wt.% glass A and **b** 10 wt.% glass B

domains are PT but there are small Al- and Si-rich crystalline regions (Fig. 11) with a composition qualitatively similar to $PbAl_2Si_2O_8$ within a Si-rich residual glass matrix. The local microstructure of the pockets of glass in the glass-PT composites is similar to that discussed by Sooksaen et al [19] who observed PT grains and a lead feldspar phase ($PbAl_2Si_2O_8$) in a glass matrix during devitrification of Glass A. Figure 12 is a BFTEM image of a sample with 10 wt.% glass B added to PT. Grains of PT (0.5 μm) with a lamellar domain structure are observed in addition to smaller grains without domain structure nucleating within regions of residual glass/second phase. The latter remains unidentified but is Al-rich (Fig. 13).

3.4 Dielectric properties

Figures 14 and 15 show the permittivity plots for samples with 3, 5 and 10 wt.% glass A and glass B, respectively, added to PT and sintered at 1,100 °C/2 h. Similar trends are observed in each plot. In general, the greater the wt.% addition of glass, the lower the peak and room temperature permittivity. Above T_c (~490 °C) in Fig. 14 (glass A addition), the ε_r follows the Curie–Wiess law as expected for a ferroelectric PT. However, in Fig. 15 (glass B addition) ε_r increases rapidly after ~530 °C. This may be due to the presence of a conducting secondary phase. The

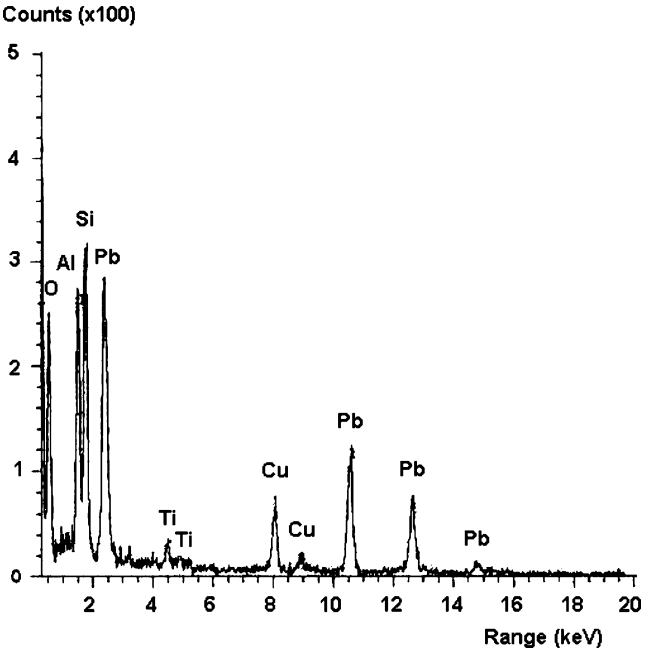

Fig. 11 EDS trace of second phase in Fig. 10

TEM image in Fig. 12 (10 wt.% glass B addition), illustrated a pocket of second phase. Boron is below the detection limit of the EDS detector but it is reasonable to assume that this phase is boron-based with a low melting

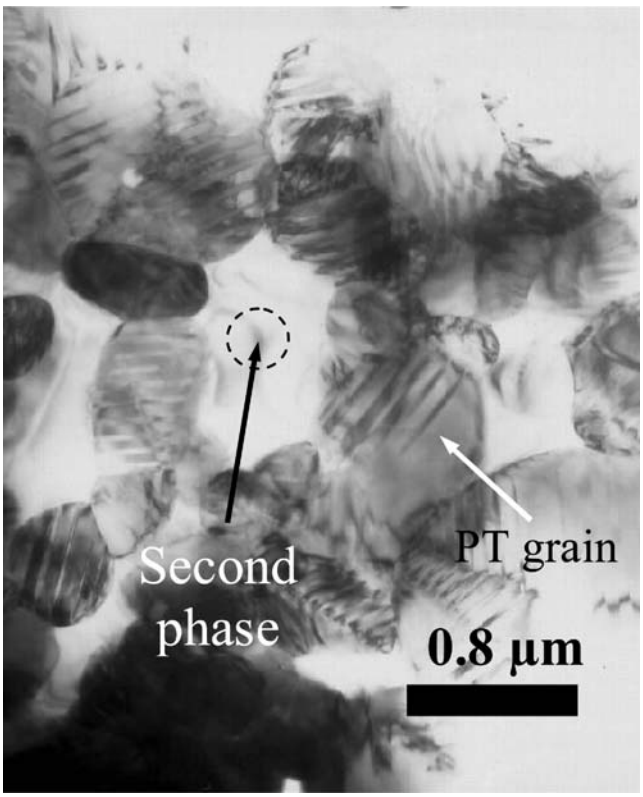

Fig. 10 BF TEM image of 10 wt.% glass A added to PT, sintered at 1,100 °C/2 h

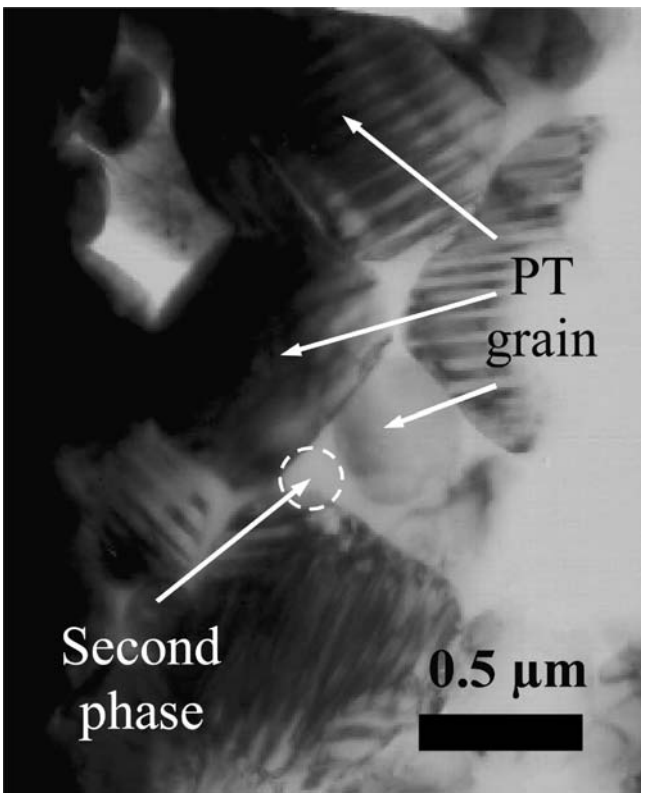

Fig. 12 BF TEM image of 10 wt.% glass B added to PT, sintered at 1,100 °C/2 h

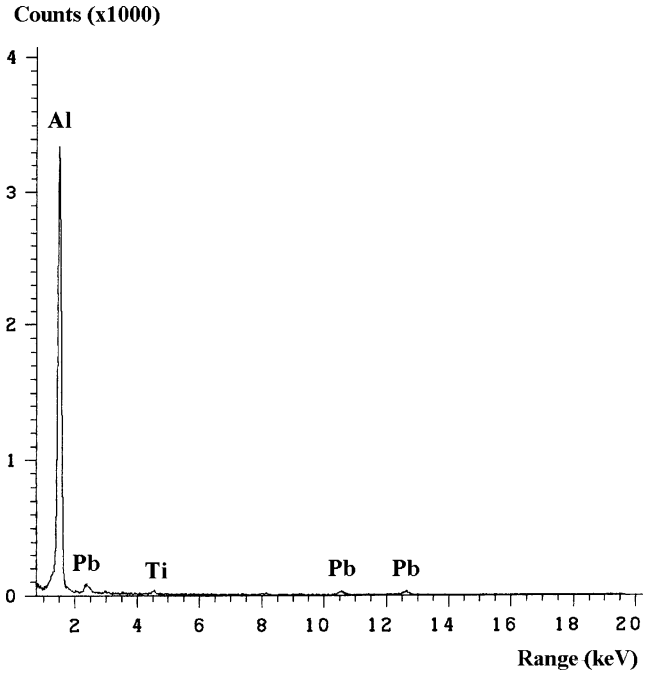

Fig. 13 EDS trace of second phase in Fig. 12

point and therefore may contribute to conduction at high temperatures. Insets in Figs. 14 and 15 are tan δ curves between 450 and 550 °C. Above ~530 °C, tan δ rises more significantly in samples with glass B addition. This agrees with a rise in permittivity, ε_r and hence may be related to the presence of conducting phase.

Careful scrutiny of Figs. 14 and 15, suggests that as the wt.% of glass addition increases, T_c decreases. In order to investigate whether this effect was real and not instrument related the impedance analyzer was calibrated against known standards and further measurements obtained.

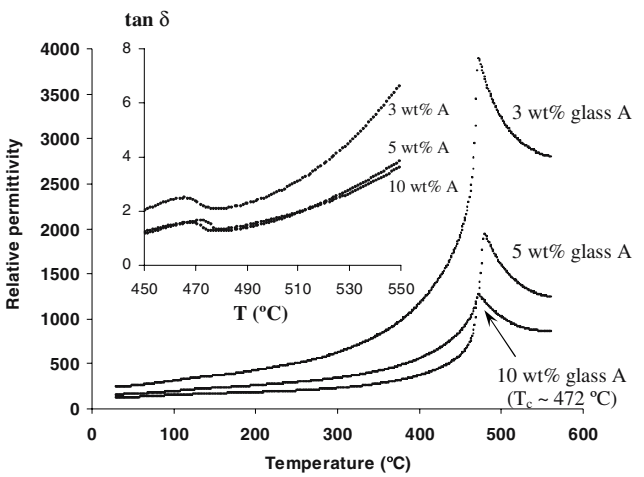

Fig. 14 Permittivity plot of 3, 5 and 10 wt.% glass A added to PT, sintered 1,100 °C/2 h. Samples were run on LCR meter at 100 kHz. Inset is tan δ curves between 450 and 550 °C

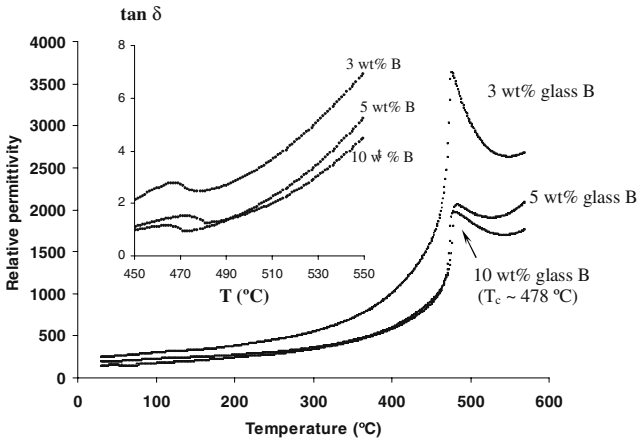

Fig. 15 Permittivity plot of 3, 5 and 10 wt.% glass B added to PT, sintered 1,100 °C/2 h. Samples were run on LCR meter at 100 kHz. Inset is tan δ curves between 450 and 550 °C

3.5 Impedance spectroscopy

The analysis on two different formalisms; Z^* complex plane plots and Z'', M'' spectroscopic plots, for all ceramic pellets at higher temperature (above 350 °C) shows the same trend. Z^* plots consist of a single semicircular arc, and the Debye peak in the Z'' and M'' are approximately at the same frequency, f_{max}. These are shown in Figs. 16 and 17, respectively. This response can be modeled on a single parallel RC element indicating that the ceramic is electrically homogeneous and the IS response is from the bulk region. There is no evidence of grain boundary impedances. The main ferroelectric phase may be modeled as a capacitor and the leakage current modeled as a resistor. At a fixed

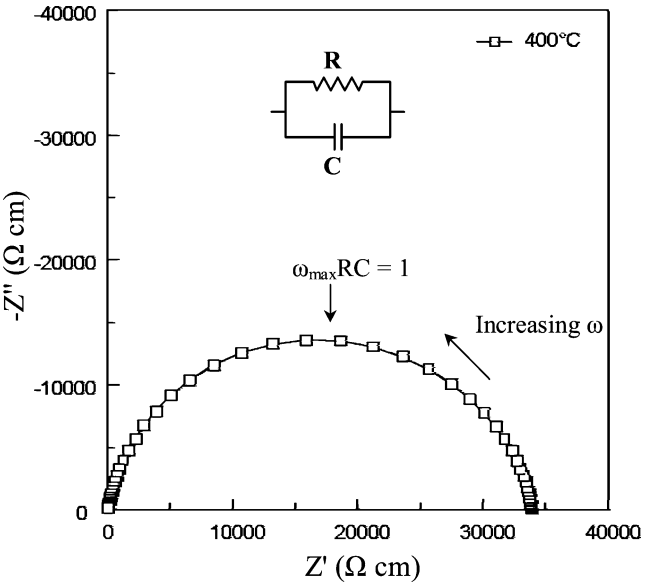

Fig. 16 Z^* plot, measured at 400 °C, of the sample with 10 wt.% glass A added, sintered at 1,100 °C/2 h

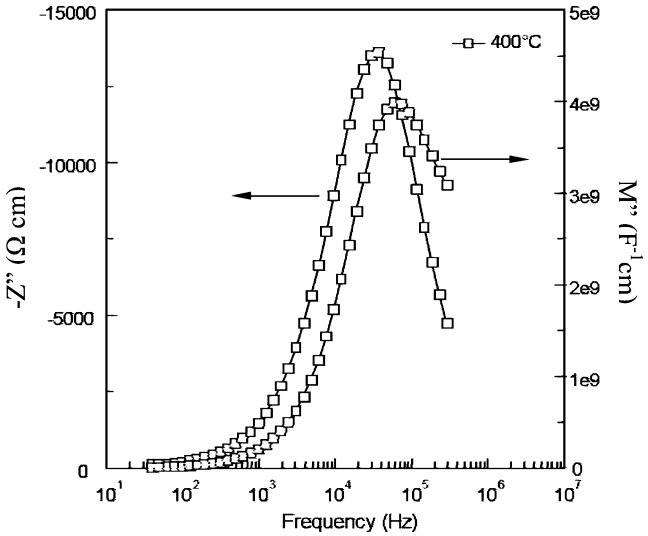

Fig. 17 Combined M'' and Z'' spectroscopic plot, measured at 400 °C, of the sample with 10 wt.% glass A added, sintered at 1,100 °C/2 h

temperature the bulk region has a characteristic time constant, τ=RC therefore $\tau=1/\omega_{max}$), where ω_{max} is the angular frequency at the maximum Z'' in Z^* plot. If f_{max} or $\omega_{max}/2\pi$ is constant or similar at the same temperature of measurement for a variety of ceramics, we can deduce that τ is constant and that there is no compositional variation associated with the samples under investigation [20].

An impedance analysis confirmed the downshift in T_c for samples sintered for 2 h but increased when sintered for longer times (Table 2). Figure 18 shows a plot of log (f_{max}) vs 1,000/T where T is temperature in Kelvin. It is shown that τ is roughly constant at each temperature for various samples, and hence the clamping effect, rather than a change in composition, is the most likely reason for the downshift in T_c by suppressing the c/a ratio which also decreases according to XRD, Fig. 3.

From the IS analysis we have also noticed an increase in sample conductivity for samples sintered for 10 h, espe-

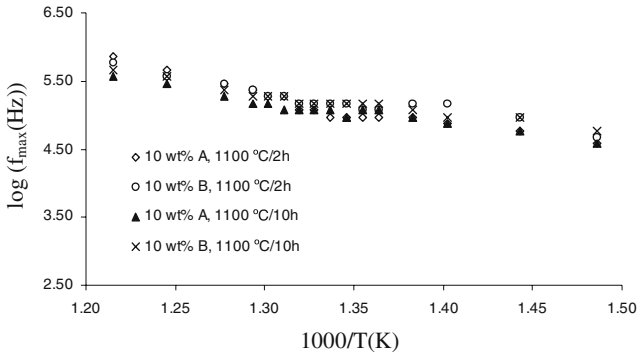

Fig. 18 log (fmax) vs (1,000/T) of samples with 10 wt.% glass addition, sintered for 2 and 10 h

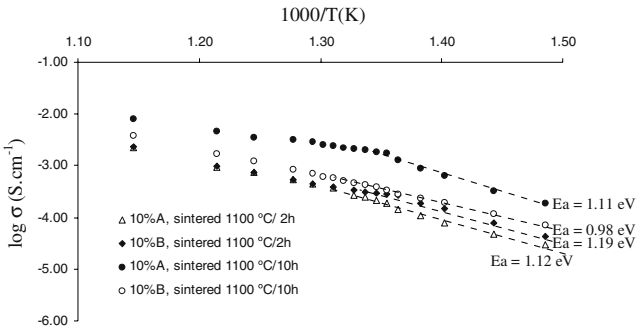

Fig. 19 Arhenius plot of conductivity for samples with 10 wt.% glass added, sintered for 2 and 10 h

cially with glass A addition. From the SEM images in Fig. 9, the grain growth mechanism, although unknown, maybe related to Pb-loss. This may link to an increase in the number of charge carriers. Figure 19 shows the activation energy, E_a, for conduction below the Curie temperature. All samples show similar E_a implying the same conduction mechanism. The electrical conductivity σ is given by $\sigma = \mu nq$ where μ is the mobility, n is the concentration of charge carriers and q is type of charge carrier. Since q and μ are fixed so an increase in the conductivity must have been from an increase in carrier concentration which may be related to Pb-loss and/or oxygen deficiency for samples sintered for extended periods at 1,100 °C.

The theoretical band gap energy for cubic PT is 3.4 eV [21, 22]. The value of E_a for intrinsic conductivity is usually represented by approximately half the value of the band gap energy. It can be said that PT has an E_a for intrinsic conduction of about 1.7 eV, assuming similar values for cubic and tetragonal PT. The values calculated from sintered glass-PT ceramics in Fig. 19 were between 0.98 and 1.19 eV (with errors associated with E_a in all cases being ±0.03) and are close to the intrinsic value of 1.7 eV. However, the discrepancy between the observed and expected values is sufficiently different to suggest the conduction behaviour in these samples is extrinsic. The extrinsic behaviour may be due to PbO/O_2 loss.

Table 2 T_c values for samples with 10 wt.% of glass addition, sintered for 2 and 10 h. Temperatures were accurate to ±3 °C.

Sintering time at 1,100 °C	Curie temperature, T_c (°C)	
	10 wt.% glass A	10 wt.% glass B
2 h	465±3	470±3
10 h	490±3	490±3

4 Conclusions

It has been demonstrated that borate- and silicate-based glasses which contain a high mol% of TiO_2 and PbO act as sintering aids for densification of $PbTiO_3$ ceramics. The density increases with increasing amount of glass addition and the level of microcracking is reduced. In general, for a given temperature and wt.% addition, the borate- gives better densification than silicate-based glass compositions. However, for 2 h sintering, PT samples containing borate-based glass show evidence of greater conductivity above T_c than the equivalent silicate system. Sintering for 10 h at 1,100 °C, results in a bimodal grain distribution. The room temperature and maximum ε_r of the lead titanate ceramics decrease along with the phase transition temperature as the wt.% glass addition increases. These effects are accompanied by a decrease in the c/a ratio which according to impedance analysis is likely to be due to clamping of the grains rather than incorporation of dopants from the glass.

In conclusion, the novelty of using PT based glasses as sintering aids from an environmental perspective is that the reduction in sintering temperature would decrease volatilisation of PbO without the addition of high dopant concentrations previously used to fabricate dense PT ceramics.

Acknowledgement The authors wish to thank the Thai Government for financial support, Heath Bagshaw and Dr Peter Korgul for their assistance with the electron microscopy.

References

1. D.L. Corker, R.W. Whatmore, E. Ringgaard, W.W. Wolny, J. Eur. Ceram. Soc. **20**, 2039 (2000)
2. K.R. Chowdary, E.C. Subbarao, Ferroelectrics **37**, 689 (1981)
3. G. Desgardin, I. Mey, B. Raveau, Am. Ceram. Soc Bull. **64**(4), 560 (1985)
4. S.K. Sarkar, M.L. Sharma, Mater. Res. Bull. **24**, 773 (1989)
5. I. Burn, J. Mater. Sci. **17**(5), 1398–1408 (1982)
6. S.F. Wang, T.C.K. Yang, Y.R. Wang, Y. Kuromitsu, Ceram. Int. **27**, 157 (2001)
7. S.Y. Cheng, S.L. Fu, C.C. Wei, Ceram. Int., **13**(4), 223 (1987)
8. M.E. Lines, A.M. Glass, *Principles and Applications of Ferroelectrics and Related Materials*, (Oxford University Press, Oxford, 1979)
9. V.R. Palkar, S. Chattopadhyay, P. Ayyub, M. Multani, S.K. Paranjape, V. Siruguri, Mater. Lett. **32**, 171 (1997)
10. V.R. Palkar, S.C. Purandare, R. Pinto, Mater. Lett. **43**, 329 (2000)
11. J.S. Wright, L.F. Francis, J. Mater. Res. **8**, 1712 (1993)
12. J. Mendiola, M.L. Calzada, P. Ramos, M.J. Martin, F. Agullo-Rueda, Journal of Thin Solid Films **315**, 195 (1998)
13. R. Tickoo, R.P. Tandon, K.K. Bamzai, P.N. Kotru, Mater. Sci. Eng., B **103**,145 (2003)
14. S.Y. Chu, T.Y. Chen, J. Eur. Ceram. Soc. **24**, 1993 (2003)
15. J.T.S. Irvine, D.C. Sinclair, A.R. West, Adv. Mater. **2**(3) 132 (1990)
16. D.C. Sinclair, A.R. West, Phys. Rev. **B39**, 13486 (1989)
17. D.C. Sinclair, A.R. West, J. Appl. Phys. **66**, 3850 (1989)
18. D.C. Sinclair, Bol. Soc. Esp. Ceram. Vidr. **34**(2), 55 (1995)
19. P. Sooksaen, I.M. Reaney, D.C. Sinclair, J. Mater. Res. **20**(5), 1316 (2005)
20. F.D. Morrison, D.C. Sinclair, A.R. West, J. Am. Ceram. Soc. **84** (3), 531 (2001)
21. J. Robertson, W.L. Warren, B.A. Tuttle, J. Appl. Phys. **78**(8), 3975 (1995)
22. W.L. Warren, J. Robertson, D. Dimos, B.A. Tuttle, G.E. Pike, D.A. Payne, Phys. Rev. B **53**, 3080 (1996)